

# Histogram of Gradient Orientations of Signal Plots applied to P300 Detection

Rodrigo Ramele<sup>1,\*</sup>, Ana Julia Villar<sup>1</sup> and Juan Miguel Santos<sup>1</sup>

<sup>1</sup>*Centro de Inteligencia Computacional, Computer Engineering Department, Instituto Tecnológico de Buenos Aires, Buenos Aires, Argentina*

Correspondence\*:

Rodrigo Ramele, C1437FBH Lavarden 315, Ciudad Autónoma de Buenos Aires, Argentina  
rramele@itba.edu.ar

## 2 ABSTRACT

3 Word Count: 4841

4 The analysis of Electroencephalographic (EEG) signals is of ulterior importance for decoding  
5 patterns that could improve the implementation of Brain Computer Interfaces (BCI). These  
6 systems are meant to provide alternative pathways to transmit volitional information which could  
7 potentially enhance the quality of life of patients affected by neurodegenerative disorders and  
8 other mental illness. Of particular interests are those which are based on the recognition of  
9 Event-Related Potentials (ERP) because they can be elicited by external stimuli and used to  
10 implement spellers, to control external devices or even avatars in virtual reality environments.  
11 This work mimics what electroencephalographers have been doing clinically, visually inspecting  
12 and categorizing phenomena within the EEG by the extraction of features from images of signal  
13 plots. It also aims to provide a framework to analyze, characterize and classify EEG signals, with  
14 a focus on the P300, an ERP elicited by the oddball paradigm of rare events. The validity of the  
15 method is shown by offline processing a public dataset of Amyotrophic Lateral Sclerosis (ALS)  
16 patients and an own dataset of healthy subjects.

17 **Keywords:** electroencephalography, histogram of gradient orientations, brain-computer interfaces, P300, SIFT, amyotrophic lateral  
18 sclerosis, naive-bayes near neighbours, waveforms

## 1 INTRODUCTION

19 Although recent advances in neuroimaging techniques, particularly radio-nuclear and radiological  
20 scanning methods (Schomer and Silva, 2010), have diminished the prospects of the traditional  
21 Electroencephalography (EEG), the advent and development of digitized devices has impelled for a  
22 revamping of this hundred years old technology. Their versatility, ease of use, temporal resolution, ease of  
23 development and production, and its proliferation as consumer devices, are pushing EEG to become the  
24 de-facto non invasive portable or ambulatory method to access and harness brain information (De Vos and  
25 Debener, 2014).

26 A key contribution to this expansion has been the field of Brain Computer Interfaces (BCI) (Wolpaw and  
27 E., 2012) which is the pursuit of the development of a new channel of communication particularly aimed to  
28 persons affected by neurodegenerative diseases.

One noteworthy aspect of this novel communication channel is the ability to transmit information from the Central Nervous System (CNS) to a computer device and from there use that information to control a wheelchair (Carlson and del R. Millan, 2013), as input to a speller application (Guger et al., 2009), in a Virtual Reality environment (Lotte et al., 2013) or as aiding tool in a rehabilitation procedure (Jure et al., 2016). The holy grail of BCI is to implement a new complete and alternative pathway to restore lost locomotion (Wolpaw and E., 2012).

EEG signals are remarkably complex and have been characterized as a multichannel non-stationary stochastic process. Additionally, they have high variability between different subjects and even between different moments for the same subject, requiring adaptive and co-adaptive calibration and learning procedures (Clerc et al., 2016). Hence, this imposes an outstanding challenge that is necessary to overcome in order to extract information from raw EEG signals.

BCI has gained mainstream public awareness with worldwide challenge competitions like Cybathlon (Riener and Seward, 2014; Novak et al., 2018) and even been broadcasted during the inauguration ceremony of the 2014 Soccer World Cup. New developments have overcome the out-of-the-lab high-bar and they are starting to be used in real world environments (Guger et al., 2017; Huggins et al., 2016). However, they still lack the necessary robustness, and its performance is well behind any other method of human computer interaction, including any kind of detection of residual muscular movement (Clerc et al., 2016).

A few works have explored the idea of exploiting the signal waveform to analyze the EEG signal. In (Alvarado-González et al., 2016) an approach based on Slope Horizontal Chain Code is presented, whereas in (Yamaguchi et al., 2009) a similar procedure was implemented based on Mathematical Morphological Analysis. The seminal work of Bandt-Pompe Permutation Entropy (Berger et al., 2017) also explores succinctly this idea as a basis to establish the time series ordinal patterns. In the article (Ramele et al., 2016), the authors introduce a method for classification of rhythmic EEG events like Visual Occipital Alpha Waves and Motor Imagery Rolandic Central  $\mu$  Rhythms using the histogram of gradient orientations of signal plots. Inspired in that work, we propose a novel application of the developed method to classify and describe transient events, particularly the P300 Event Related Potential. The proposed approach is based on the waveform analysis of the shape of the EEG signal, but using histogram of gradient orientations. The method is built by mimicking what traditionally electroencephalographers have been performing for almost a century as it is described in (Hartman, 2005): visually inspecting raw signal plots.

This paper reports a method to, (1) describe a procedure to capture the shape of a waveform of an ERP component, the P300, using histograms of gradient orientations extracted from images of signal plots, and (2) outline the way in which this procedure can be used to implement an offline P300-based BCI Speller application. Its validity is verified by offline processing two datasets, one of data from ALS patients and another one from data of healthy subjects.

This article unfolds as follows: Section 2.1 is dedicated to explain the Feature Extraction method based on Histogram of Gradient Orientations of the Signal Plot: Section 2.1.1 shows the preprocessing pipeline, Section 2.1.3 describes the image generation of the signal plot, Section 2.1.4 presents the feature extraction procedure while Section 2.1.5 introduces the Speller Matrix Letter Identification procedure. In Section 2.2, the experimental protocol is expounded. Section 3 shows the results of applying the proposed technique. In the final Section 4 we expose our remarks, conclusions and future work.

## 2 MATERIALS AND METHODS

The P300 (Farwell and Donchin, 1988; Knuth et al., 2006) is a positive deflection of the EEG signal which occurs around 300 ms after the onset of a rare and deviant stimulus that the subject is expected to attend. It is produced under the oddball paradigm (Wolpaw and E., 2012) and it is consistent across different subjects. It has a lower amplitude ( $\pm 5\mu V$ ) compared to basal EEG activity, reaching a Signal to Noise Ratio (SNR) of around  $-15$  db estimated based on the amplitude of the P300 response signal divided by the standard deviation of the background EEG activity (Hu et al., 2010). This signal can be used to implement a speller application by means of a Speller Matrix (Farwell and Donchin, 1988). This matrix is composed of 6 rows and 6 columns of numbers and letters. The subject can focus on one character of the matrix. Fig. 1 shows an example of the Speller Matrix used in the OpenVibe open source software (Renard et al., 2010), where the flashes of rows and columns provide the deviant stimulus required to elicit this physiological response. Each time a row or a column that contains the desired letter flashes, the corresponding synchronized EEG signal should also contain the P300 signature and by detecting it, the selected letter can be identified.

### 2.1 Feature Extraction from Signal Plots

In this section, the signal preprocessing, the method for generating images from signal plots, the feature extraction procedure and the Speller Matrix identification are described. Fig. 3 shows a scheme of the entire process.

#### 2.1.1 Preprocessing Pipeline

The data obtained by the capturing device is digitalized and a multichannel EEG signal is constructed.

The 6 rows and 6 columns of the Speller Matrix are intensified providing the visual stimulus. The twelve locations  $l$  are randomly permuted and they conform an intensification sequence. The whole set of twelve intensifications is repeated  $ka$  times.

- **Signal Enhancement:** The preprocessing stage consists of the enhancement of the SNR of the P300 pattern above the level of basal EEG. The pipeline starts by applying a notch filter to the raw digital signal, a 4th degree 10 Hz lowpass Butterworth filter and finally a decimation with a Finite Impulse Response (FIR) filter of order 30 from the original sampling frequency down to 16 Hz (Krusienski et al., 2006).
- **Artifact Removal:** For every complete sequence of 12 intensifications of 6 rows and 6 columns, a basic artifact elimination procedure is implemented by removing the entire sequence when any signal deviates above/bellow  $\pm 70\mu V$ .
- **Segmentation:** For each of the 12 intensifications, a segment  $S_i^l$  of a window of  $t_{max}$  seconds of the multichannel signal is extracted, starting from the stimulus onset, corresponding to each row/column intensification  $l$  and to the intensification sequence  $i$ . Segments are rearranged corresponding to row flickering, labeled 1-6, whereas those corresponding to column flickering are labeled 7-12. Two of these segments should contain the P300 ERP signature time-locked to the flashing stimulus, one for the row, and one for the column.
- **Signal Averaging:** The P300 ERP is deeply buried under background EEG so the traditional approach to identify it is by point-to-point averaging the time-locked stacked signal segments. Hence the values which are not related to, and not time-locked to the onset of the stimulus are canceled out (Liang and Bougrain, 2008).

109 This last step determines the operation of any P300 Speller. In order to obtain an improved signal in  
 110 terms of its SNR, repetitions of the sequence of row/column intensification are necessary. And, at the same  
 111 time, as long as more repetitions are needed, the ability to transfer information faster is diminished, so  
 112 there is a trade-off that must be acutely determined.

### 113 2.1.2 Ensemble Average

114 The procedure to obtain the point-to-point averaged signal goes as follows:

- 115 1. Highlight randomly the rows and columns from the matrix. There is one row and one column that  
 116 should match the letter selected by the subject.
- 117 2. Repeat step 1  $k_a$  times, obtaining the segments  $S_1^l(n, c), \dots, S_{k_a}^l(n, c)$ , of the EEG signal where  
 118 the variables  $n \in \{1, \dots, n_{max}\}$  and  $c \in \{1, 2, \dots, C\}$  correspond to sample points and channel,  
 119 respectively. The parameter  $C$  is the number of available EEG channels whereas  $n_{max} = F_s \cdot t_{max}$  is  
 120 the segment length and  $F_s$  is the sampling frequency. The parameter  $k_a$  is the number of repetitions of  
 121 intensifications and it is an input parameter of the algorithm.
- 122 3. Compute the Ensemble Average by

$$x^l(n, c) = \frac{1}{k_a} \sum_{i=1}^{k_a} S_i^l(n, c), n \in \{1, \dots, n_{max}\}, c \in \{1, \dots, C\} \quad (1)$$

123 for each row and column on the Speller Matrix.

### 124 2.1.3 Signal Plotting

125 Averaged signal segments are standardized and scaled by

$$\tilde{x}^l(n, c) = \left\lceil \gamma \cdot \frac{(x^l(n, c) - \bar{x}^l(c))}{\hat{\sigma}^l(c)} \right\rceil, n \in \{1, \dots, n_{max}\}, c \in \{1, 2, \dots, C\} \quad (2)$$

where  $\gamma > 0$  is an input parameter of the algorithm and it is related to the image scale. In addition,  $x^l(n, c)$   
 is the point-to-point averaged multichannel EEG signal for the sample point  $n$  and for channel  $c$ . Lastly,

$$\bar{x}^l(c) = \frac{1}{n_{max}} \sum_{n=1}^{n_{max}} x^l(n, c)$$

and

$$\hat{\sigma}^l(c) = \left( \frac{1}{n_{max} - 1} \sum_{n=1}^{n_{max}} (x^l(n, c) - \bar{x}^l(c))^2 \right)^{\frac{1}{2}}$$

126 are the mean and estimated standard deviation of  $x^l(n, c), n \in \{1, \dots, n_{max}\}$ , for each channel  $c$ .

127 Consequently, for a pixel  $(z_1, z_2)$ , the image  $I^l$  is constructed according to

$$I^{(l,c)}(z_1, z_2) = \begin{cases} 255 & \text{if } z_1 = \gamma \cdot n; z_2 = \tilde{x}^l(n, c) + z^l(c) \\ 0 & \text{otherwise} \end{cases} \quad (3)$$

where  $(z_1, z_2) \in \mathbb{N} \times \mathbb{N}$  iterate over the width (based on the length of the signal segment) and height (based on the peak-to-peak amplitude) of the newly created image,  $n \in \{1, \dots, n_{max}\}$  and  $c \in \{1, 2, \dots, C\}$ . The values  $z^l(c)$ ,  $c \in \{1, 2, \dots, C\}$  are the location on the image where the signal's zero value has to be located in order to fit the entire signal within the image for each  $c$ :

$$z^l(c) = \left\lfloor \frac{\max_n \tilde{x}^l(n, c) - \min_n \tilde{x}^l(n, c)}{2} \right\rfloor - \left\lfloor \frac{\max_n \tilde{x}^l(n, c) + \min_n \tilde{x}^l(n, c)}{2} \right\rfloor \quad (4)$$

where the minimization and maximization are carried out for  $n$  varying between  $1 \leq n \leq n_{max}$ .

In order to complete the plot from the pixels, the Bresenham (Bresenham, 1965; Ramele et al., 2016) algorithm is used to interpolate straight lines between each pair of consecutive pixels.

#### 2.1.4 Feature Extraction: Histogram of Gradient Orientations

For each generated image  $I^{(l,c)}$ , a keypoint  $\mathbf{kp}$  is placed on a pixel  $(x_{kp}, y_{kp})$  over the image plot and a window around the keypoint is considered. A local image patch of size  $X_p \times X_p$  pixels is constructed by dividing the window in 16 blocks of size  $3s$  each one, where  $s$  is the scale of the local patch and it is an input parameter of the algorithm. It is arranged in a  $4 \times 4$  grid and the pixel  $\mathbf{kp}$  is the patch center, thus  $X_p = 12s$  pixels.

A local representation of the signal shape within the patch can be described by obtaining the gradient orientations on each of the 16 blocks and creating a histogram of gradients. This technique is based on Lowe's SIFT (Lowe, 2004) method, and it is biomimetically inspired in how the visual cortex detects shapes by analyzing orientations (Edelman et al., 1997). In order to calculate the histogram, the interval  $[0 - 360]$  of possible angles is divided in 8 bins, each one at 45 degrees.

Hence, for each spacial bin  $i, j \in \{0, 1, 2, 3\}$ , corresponding to the indexes of each block  $B_{i,j}$ , the orientations are accumulated in a 3-dimensional histogram  $h$  through the following equation:

$$h(\theta, i, j) = 3s \sum_{\mathbf{p} \in I} w_{\text{ang}}(\angle J(\mathbf{p}) - \theta) w_{ij} \left( \frac{\mathbf{p} - \mathbf{kp}}{3s} \right) |J(\mathbf{p})| \quad (5)$$

where  $\mathbf{p}$  is a pixel from the image  $I$ ,  $\theta$  is the angle bin with  $\theta \in \{0, 45, 90, 135, 180, 225, 270, 315\}$ ,  $|J(\mathbf{p})|$  is the norm of the gradient vector in the pixel  $\mathbf{p}$  and it is computed using finite differences and  $\angle J(\mathbf{p})$  is the angle of the gradient vector. The scalar  $w_{\text{ang}}(\cdot)$  and vector  $w_{ij}(\cdot)$  functions are linear interpolations used by Lowe (2004) and Vedaldi and Fulkerson (2010) to provide a weighting contribution to eight adjacent bins. They are calculated as

$$w_{ij}(\mathbf{v}) = w(v_x - x_i)w(v_y - y_j)/i, j \in \{0, 1, 2, 3\} \quad (6)$$

$$w_{\text{ang}}(\alpha) = \sum_{r \in [-1, 1]} w\left(\frac{8\alpha}{2\pi} + 8r\right) \quad (7)$$

where  $x_i$  and  $y_i$  are the spatial bin centers located in  $x_i, y_i \in \{-\frac{3}{2}, -\frac{1}{2}, \frac{1}{2}, \frac{3}{2}\}$ ,  $\mathbf{v} = (v_x, v_y)$  is a dummy vector variable and  $\alpha$  a dummy scalar variable. On the other hand,  $r$  is an integer that can vary freely

155 between  $[-1, 1]$  which allows the argument  $\alpha$  to be unconstrained in terms of its values in radians. The  
 156 interpolating function  $w(\cdot)$  is defined as:

$$w(z) = \max(0, |z| - 1) \quad (8)$$

157 These binning functions conform a trilinear interpolation that has a combined effect of sharing the  
 158 contribution of each oriented gradient between their eight adjacent bins in a tridimensional cube in the  
 159 histogram space, and zero everywhere else.

160 Lastly, the fixed value of 3 is a magnification factor which corresponds to the number of pixels per each  
 161 block when  $s = 1$ . As the patch has 16 blocks and 8 bin angles are considered, for each location  $l$  and  
 162 channel  $c$  a feature called *descriptor*  $d^{(l,c)}$  of 128 dimension is obtained.

163 Fig. 2 shows an example of a patch and a scheme of the histogram computation. In (A) a plot of the  
 164 signal and the patch centered around the keypoint is shown. In (B) the possible orientations on each patch  
 165 are illustrated. Only the upper-left four blocks are visible. The first eight orientations of the first block, are  
 166 labeled from 1 to 8 clockwise. The orientations of the second block  $B_{1,2}$  are labeled from 9 to 16. This  
 167 labeling continues left-to-right, up-down until the eight orientations for all the sixteen blocks are assigned.  
 168 They form the corresponding *kp*-descriptor of 128 coordinates. Finally, in (C) an enlarged image plot is  
 169 shown where the oriented gradient vector for each pixel can be seen.

## 170 2.1.5 Speller Matrix letter Identification

### 171 2.1.5.1 P300 ERP Extraction

172 Segments corresponding to row flickering are labeled 1-6, whereas those corresponding to column  
 173 flickering are labeled 7-12. The extraction process has the following steps:

174 First highlight randomly the rows and columns from the matrix and obtain the Ensemble Average as  
 175 detailed in steps 1, 2 and 3 in Section 2.1.2.

- 176 • **Step A:** Plot the signals  $\tilde{x}^l(n, c)$ ,  $n \in \{1, \dots, n_{max}\}$ ,  $c \in \{1, \dots, C\}$ , according Section 2.1.3 in order  
 177 to generate the images  $I^{(l,c)}$  for rows and columns.
- 178 • **Step B:** Obtain the descriptors  $d^{(l,c)}$  for rows and columns from  $I^{(l,c)}$  in accordance to the method  
 179 described in Section 2.1.4.

### 180 2.1.5.2 Calibration

181 A trial, as defined by the BCI2000 platform (Schalk et al., 2004), is every attempt to select just one letter  
 182 from the speller. A set of trials is used for calibration and once the calibration is complete it can be used to  
 183 identify new letters from new trials.

184 During the calibration phase, two descriptors  $d^{(l,c)}$  are extracted for every available channel for the  
 185 calibration trials, corresponding a previously known chosen letter. These descriptors are the P300 templates,  
 186 grouped together in a template set called  $T$ . The set is constructed using the steps described in Section  
 187 2.1.2 and the steps A and B of the P300 ERP extraction process.

188 Additionally, the best performing channel,  $bpc$  is identified based on the the channel where the best letter  
 189 recognition rate is obtained.

### 190 2.1.5.3 Letter identification

191 In order to identify the selected letter, the template set  $T$  is used as a database. Thus, new descriptors are  
192 computed and they are compared against the descriptors belonging to the calibration template set  $T$ .

193 • **Step C:** Match to the calibration template  $T$  by computing

$$row = \arg \min_{l \in \{1, \dots, 6\}} \sum_{q \in N_T(d^{(l, bpc)})} \|q - d^{(l, bpc)}\|_2^2 \quad (9)$$

194 and

$$col = \arg \min_{l \in \{7, \dots, 12\}} \sum_{q \in N_T(d^{(l, bpc)})} \|q - d^{(l, bpc)}\|_2^2 \quad (10)$$

195 where  $N_T(d^l)$  is defined as  $N_T(d_u^l) = \{d \in T / \text{is the } k\text{-nearest neighbor of } d^l\}$  for the best performing  
196 channel. This set is obtained by sorting all the elements in  $T$  based on euclidean distances between  
197 them and  $d^l$ , choosing the parameter  $k$  with smaller values. This procedure is based on the k-NBNN  
198 algorithm (Boiman et al., 2008).

199 By computing the aforementioned equations, the letter of the matrix can be determined from the intersection  
200 of the row  $row$  and column  $col$ . Figure 3 shows a scheme of this process.

## 201 2.2 Experimental Protocol

202 To verify the validity of the proposed framework and method, the public dataset 008-2014 (Riccio et al.,  
203 2013) published on the BNCI-Horizon website (Brunner et al., 2014) by IRCCS Fondazione Santa Lucia,  
204 is used. Additionally, an own dataset with the same experimental conditions is generated. Both of them are  
205 utilized to perform an offline BCI Simulation to decode the spelled words from the provided signals.

206 The algorithm is implemented using VLFeat (Vedaldi and Fulkerson, 2010) Computer Vision libraries on  
207 MATLAB V2014a (Mathworks Inc., Natick, MA, USA).

208 In the following sections the characteristics of the datasets and parameters of the identification algorithm  
209 are described.

### 210 2.2.1 P300 ALS Public Dataset

211 The experimental protocol used to generate this dataset is explained in (Riccio et al., 2013) but can  
212 be summarized as follows: 8 subjects with confirmed diagnoses but on different stages of ALS disease,  
213 were recruited and accepted to perform the experiments. The Visual P300 detection task designed for this  
214 experiment consisted of spelling 7 words of 5 letters each, using the traditional P300 Speller Matrix (Farwell  
215 and Donchin, 1988). The flashing of rows and columns provide the deviant stimulus required to elicit this  
216 physiological response. The first 3 words are used for calibration and the remaining 4 words, for testing  
217 with visual feedback. A trial, as defined by the BCI2000 platform (Schalk et al., 2004), is every attempt to  
218 select a letter from the speller. It is composed of signal segments corresponding to  $k_a = 10$  repetitions of  
219 flashes of 6 rows and  $k_a = 10$  repetitions of flashes of 6 columns of the matrix, yielding 120 repetitions.  
220 Flashing of a row or a column is performed for 0.125 s, following by a resting period (i.e. inter-stimulus  
221 interval) of the same length. After 120 repetitions an inter-trial pause is included before resuming with the  
222 following letter.



The recorded dataset was sampled at 256 Hz and it consisted of a scalp multichannel EEG signal for electrode channels Fz, Cz, Pz, Oz, P3, P4, PO7 and PO8, identified according to the 10-20 International System, for each one of the 8 subjects. The recording device was a research-oriented digital EEG device (g.Mobilab, g.Tec, Austria) and the data acquisition and stimuli delivery were handled by the BCI2000 open source software (Schalk et al., 2004).

In order to assess and verify the identification of the P300 response, subjects are instructed to perform a copy-spelling task. They have to fix their attention to successive letters for copying a previously determined set of words, in contrast to a free-running operation of the speller where each user decides on its own what letter to choose.

### 2.2.2 P300 for healthy subjects

We replicate the same experiment on healthy subjects (Ramele et al., 2017) using a wireless digital EEG device (g.Nautilus, g.Tec, Austria). The experimental conditions are the same as those used for the previous dataset, as detailed in section 2.2.1.

Participants are recruited voluntarily and the experiment is conducted anonymously in accordance with the Declaration of Helsinki published by the World Health Organization. No monetary compensation is handed out and all participants agree and sign a written informed consent. This study is approved by the *Departamento de Investigación y Doctorado, Instituto Tecnológico de Buenos Aires (ITBA)*. All healthy subjects have normal or corrected-to-normal vision and no history of neurological disorders. The experiment is performed with 8 subjects, 6 males, 2 females, 6 right-handed, 2 left-handed, average age 29.00 years, standard deviation 11.56 years, range 20-56 years.

EEG data is collected in a single recording session. Participants are seated in a comfortable chair, with their vision aligned to a computer screen located one meter in front of them. The handling and processing of the data and stimuli is conducted by the OpenVibe platform (Renard et al., 2010).

Gel-based active electrodes (g.LADYbird, g.Tec, Austria) are used on the same locations Fz, Cz, Pz, Oz, P3,P4, PO7 and PO8. Reference is set to the right ear lobe and ground is preset as the AFz position. Sampling frequency is slightly different, and is set to 250 Hz, which is the closest possible to the one used with the other dataset.

### 2.2.3 Parameters

The patch size is  $X_P = 12s \times 12s$  pixels, where  $s$  is the scale of the local patch and it is an input parameter of the algorithm. The P300 event can have a span of 400 ms and its amplitude can reach  $10\mu V$  (Rao, 2013). Hence it is necessary to utilize a signal segment of size  $t_{max} = 1$  second and a size patch  $X_P$  that could capture an entire transient event. With this purpose in consideration, the  $s$  value election is essential.

We propose the Equations 11 and 12 to compute the scale value in horizontal and vertical directions, respectively.

$$s_x = \frac{\lambda \cdot F_s}{12} \cdot \gamma \quad (11)$$

$$s_y = \frac{\Delta\mu V}{12} \cdot \gamma \quad (12)$$

where  $\lambda$  is the length in seconds covered by the patch,  $F_s$  is the sampling frequency of the EEG signal (downsampled to 16 Hz) and  $\Delta\mu V$  corresponds to the amplitude in microvolts that can be covered by the



height of the patch. The geometric structure of the patch forces a squared configuration, then we discerned that by using  $s = s_x = s_y = 3$  and  $\gamma = 4$ , the local patch and the descriptor can identify events of  $9 \mu V$  of amplitude, with a span of  $\lambda = 0.56$  seconds. This also determines that 1 pixel represents  $\frac{1}{\gamma} = \frac{1}{4} \mu V$  on the vertical direction and  $\frac{1}{F_s \cdot \gamma} = \frac{1}{64}$  seconds on the horizontal direction. Descriptors  $k_p$  are located at  $(x_{kp}, y_{kp}) = (0.55 F_s \cdot \gamma, z(c)) = (35, z(c))$  for the corresponding channel  $c$  (see Eq. 4). In this way the whole transient event is captured. Figure 4 shows a patch of a signal plot covering the complete amplitude (vertical direction) and the complete span of the signal event (horizontal direction).

Lastly, the number of channels  $C$  is equal to 8 for both datasets, and the number of intensification sequences  $k_a$  is statically assigned to 10. The parameter  $k$  used to construct the set  $N_T(d^l)$  is assigned to  $k = 7$ , which was found empirically to achieve better results. In addition, the norm used on Equations 9 and 10 is the cosine norm, and descriptors are normalized to  $[-1, 1]$ .

### 3 RESULTS

Table 2 shows the results of applying the algorithm to the subjects of the public dataset of ALS patients. The percentage of correctly spelled letters is calculated while performing an offline BCI Simulation. From the seven words for each subject, the first three are used as calibration, and the remaining four for testing. The best performing channel is informed as well. The target ratio is 1 : 36; hence chance level is 2.8%. It can be observed that the best performance of the letter identification method is reached in various channels depending on the subject been studied.

The Information Transfer Rate (ITR), or Bit Transfer Rate (BTR), in the case of reactive BCIs (Wolpaw and E., 2012) depends on the amount of signal averaging required to transmit a valid and robust selection. Fig. 5 shows the performance curves for varying intensification sequences. It can be noticed that the percentage of correctly identified letters depends on the number of intensification sequences  $k_a$  that are used to obtain the averaged signal. Moreover, when the number of intensification sequences tend to 1, which corresponds to single-intensification character recognition, the performance is reduced. As mentioned before, the SNR of the P300 obtained from only one segment is very low and the shape of its P300 component is not very well defined.

In Table 3 results obtained for 8 healthy subjects are shown. The obtained performance were slightly inferior than those obtained for ALS patients but well above chance level.

For comparison, in both tables results for Rate Character Recognition with the SWLDA algorithm are added. The feature was obtained by concatenating all the channels (Krusienski et al., 2006) and the SWLDA algorithm is used in accordance to the publishers of the ALS dataset (Riccio et al., 2013). The rate obtained for both datasets is slightly improved in relation to SWLDA. Additionally Tables ?? and ?? show the obtained performance for the algorithms Permutation Entropy PE and SVM support vector machine. These algorithms also works on a channel by channel basis and particularly PE extracts information from the waveform.

The P300 ERP consists of two overlapping components: the P3a and P3b, the former with frontocentral distribution while the later stronger on centroparietal region (Polich, 2007). Hence, the standard practice is to find the stronger response on the central channel Cz (Riccio et al., 2013). However, Krusienski et al. (2006) show that the response may also arise in occipital regions. We found that by analyzing only the waveforms, occipital channels PO8 and PO7 show higher performances for some subjects.

As subjects have varying *latencies* and *amplitudes* of their P300 components, they also have a varying stability of the *shape* of the generated ERP (Nam et al., 2010). Figure 6 shows the P300 templates patches for patients 8 and 3 from the dataset of ALS patients. It can be discerned that in coincidence with the performance results, the P300 signature is more clear and consistent for subject 8 (A) while for subject 3 (B) the characteristic pattern is more difficult to perceive.

Additionally, the stability of the P300 component waveform has been extensively studied in patients with ALS (Sellers et al., 2006; Madarame et al., 2008; Nijboer and Broermann, 2009; Mak et al., 2012; McCane et al., 2015) where it was found that these patients have a stable P300 component, which were also sustained across different sessions. In line with these results we do not find evidence of a difference in terms of the performance obtained for the group of patients with ALS and the healthy group of volunteers. Particularly, the best performance is obtained for a subject from the ALS dataset for which, based on visual observation, the shape of they P300 component is consistently identified.

It is important to remark that when applied to binary images obtained from signal plots, the feature extraction method described in Section 2.1.4 generates sparse descriptors. Under this subspace we found that using the cosine metric yielded a significant performance improvement. On the other hand, the unary classification scheme based on the NBN algorithm proved very beneficial for the P300 Speller Matrix. This is due to the fact that this approach solves the unbalance dataset problem which is inherent to the oddball paradigm (Tibon and Levy, 2015).

## 4 DISCUSSION

Among other applications of Brain Computer Interfaces, the goal of the discipline is to provide communication assistance to people affected by neuro-degenerative diseases, who are the most likely population to benefit from BCI systems and EEG processing and analysis.

In this work, a method to detect transient P300 components from EEG signals based on their waveform characterization in digital time-space, is presented. Additionally, its validity is evaluated using a public dataset of ALS patients and an own dataset of healthy subjects.

This method has the advantage that shapes of waveforms can be analyzed in an objective way. We observed that the shape of the P300 component is more stable in occipital channels, where the performance for identifying letters is higher. We additionally verified that ALS P300 signatures are stable in comparison to those of healthy subjects. Further work should be conducted over larger samples to cross-check the validity of these results.

We believe that the use of descriptors based on histogram of gradient orientation, presented in this work, can also be utilized for deriving a shape metric in the space of the P300 signals which can complement other metrics based on time-domain as those defined by Mak et al. (2012). It is important to notice that the analysis of waveform shapes is usually performed in a qualitative approach based on visual inspection (Sellers et al., 2006).

The goal of this work is to answer the question if a P300 component could be solely determined by inspecting automatically their waveforms. We conclude affirmatively, though two very important issues still remain:

First, the stability of the P300 in terms of its shape is crucial: the averaging procedure, montages, the signal to noise ratio and spatial filters all of them are non-physiological factors that affect the stability of the shape of the P300 ERP. We tested a preliminary approach to assess if the morphological shape of

the P300 can be stabilized by applying different latency shifts to segments and we verified that there is a better performance when a correct segment alignment is applied. We also applied Dynamic Time Warping (DTW) (Casarotto et al., 2005) but we were unable to find a substantial improvement. Further work to study the stability of the P300 signature component needs to be addressed.

The second problem is the amplitude variation of the P300. We propose a solution by standardizing the signal, shown in Eq. 2. It has the effect of normalizing the peak-to-peak amplitude, moderating its variation. It has also the advantage of reducing noise that was not reduced by the averaging procedure. It is important to remark that the averaged signal variance depends on the number of segments used to compute it (Van Drongelen, 2006). The standardizing process converts the signal to unit signal variance which makes it independent of the number  $k_a$  of signals averaged. Although this is initially an advantageous approach, the standardizing process reduces the amplitude of any significant P300 complex diminishing its automatic interpretation capability.

In our opinion, the best benefit of the presented method is that a closer collaboration with physicians can be fostered, since this procedure intent to imitate human visual observation. Automatic classification of patterns in EEG that are specifically identified by their shapes like K-Complex, Vertex Waves, Positive Occipital Sharp Transient (Hartman, 2005) are a prospect future work to be considered. We are currently working in unpublished material analyzing K-Complex components that could eventually provide assistance to physicians to locate these EEG patterns, specially in long recording periods, frequent in sleep research. Additionally, it can be used for artifact removal which is performed on many occasions by visually inspecting signals. This is due to the fact that the descriptors are a direct representation of the shape of signal waveforms. In line with these applications, it can be used to build a database (Chavarriaga et al., 2017) of quantitative representations of waveforms and improve atlases (Hartman, 2005), which are currently based on qualitative descriptions of signal shapes.

## CONFLICT OF INTEREST STATEMENT

The authors declare that the research was conducted in the absence of any commercial or financial relationships that could be construed as a potential conflict of interest.

## AUTHOR CONTRIBUTIONS

This work is part of the PhD thesis of RR which is directed by JS and codirected by AV.

## FUNDING

This project was supported by the ITBACyT-15 funding program issued by ITBA University from Buenos Aires, Argentina.

## REFERENCES

- Alvarado-González, M., Garduño, E., Bribiesca, E., Yáñez-Suárez, O., and Medina-Bañuelos, V. (2016). P300 Detection Based on EEG Shape Features. *Computational and Mathematical Methods in Medicine*, 1–14doi:10.1155/2016/2029791
- Berger, S., Schneider, G., Kochs, E., and Jordan, D. (2017). Permutation Entropy: Too Complex a Measure for EEG Time Series? *Entropy* 2017, Vol. 19, Page 692 19, 692. doi:10.3390/E19120692

- Boiman, O., Shechtman, E., and Irani, M. (2008). In defense of nearest-neighbor based image classification. *26th IEEE Conference on Computer Vision and Pattern Recognition, CVPR* doi:10.1109/CVPR.2008.4587598
- Bresenham, J. E. (1965). Algorithm for computer control of a digital plotter. *IBM Systems Journal* 4, 25–30
- Brunner, C., Blankertz, B., Cincotti, F., Kübler, A., Mattia, D., Miralles, F., et al. (2014). BNCI Horizon 2020 – Towards a Roadmap for Brain / Neural Computer Interaction. *Lecture Notes in Computer Science* 8513, 475–486
- Carlson, T. and del R. Millan, J. (2013). Brain-controlled wheelchairs: A robotic architecture. *IEEE Robotics & Automation Magazine* 20, 65–73. doi:10.1109/MRA.2012.2229936
- Casarotto, S., Bianchi, A., Cerutti, S., and Chiarenza, G. (2005). Dynamic time warping in the analysis of event-related potentials. *IEEE Engineering in Medicine and Biology Magazine* 24, 68–77. doi:10.1109/EMEMB.2005.1384103
- Chavarriaga, R., Fried-Oken, M., Kleih, S., Lotte, F., and Scherer, R. (2017). Heading for new shores! Overcoming pitfalls in BCI design. *Brain-Computer Interfaces* 4, 60–73. doi:10.1080/2326263X.2016.1263916
- Clerc, M., Bougrain, L., and Lotte, F. (2016). *Brain-computer interfaces, Technology and applications 2(Cognitive Science)* (ISTE Ltd. and Wiley)
- De Vos, M. and Debener, S. (2014). Mobile EEG: Towards brain activity monitoring during natural action and cognition. *International Journal of Psychophysiology* 91, 1–2. doi:10.1016/j.ijpsycho.2013.10.008
- Edelman, S., Intrator, N., and Poggio, T. (1997). Complex cells and object recognition
- Farwell, L. A. and Donchin, E. (1988). Talking off the top of your head: toward a mental prosthesis utilizing event-related brain potentials. *Electroencephalography and clinical neurophysiology* 70, 510–23
- Guger, C., Allison, B. Z., and Lebedev, M. A. (2017). Introduction. In *Brain Computer Interface Research: A State of the Art Summary 6* (Springer, Cham). 1–8. doi:10.1007/978-3-319-64373-1\_1
- Guger, C., Daban, S., Sellers, E., Holzner, C., Krausz, G., Carabalona, R., et al. (2009). How many people are able to control a P300-based brain-computer interface (BCI)? *Neuroscience Letters* 462, 94–98. doi:10.1016/j.neulet.2009.06.045
- Hartman, a. L. (2005). *Atlas of EEG Patterns*, vol. 65 (Lippincott Williams & Wilkins). doi:10.1212/01.wnl.0000174180.41994.39
- Hu, L., Mouraux, A., Hu, Y., and Iannetti, G. D. (2010). A novel approach for enhancing the signal-to-noise ratio and detecting automatically event-related potentials (ERPs) in single trials. *NeuroImage* 50, 99–111. doi:10.1016/j.neuroimage.2009.12.010
- Huggins, J. E., Alcaide-Aguirre, R. E., and Hill, K. (2016). Effects of text generation on P300 brain-computer interface performance. *Brain-Computer Interfaces* 3, 112–120. doi:10.1080/2326263X.2016.1203629
- Jure, F., Carrere, L., Gentiletti, G., and Tabernig, C. (2016). BCI-FES system for neuro-rehabilitation of stroke patients. *Journal of Physics: Conference Series* 705, 1–8. doi:10.1088/1742-6596/705/1/012058
- Knuth, K. H., Shah, A. S., Truccolo, W. A., Ding, M., Bressler, S. L., and Schroeder, C. E. (2006). Differentially variable component analysis: Identifying multiple evoked components using trial-to-trial variability. *Journal of Neurophysiology* 95, 3257–3276. doi:10.1152/jn.00663.2005
- Krusienski, D. J., Sellers, E. W., Cabestaing, F., Bayouth, S., McFarland, D. J., Vaughan, T. M., et al. (2006). A comparison of classification techniques for the P300 Speller. *Journal of Neural Engineering* 3, 299–305. doi:10.1088/1741-2560/3/4/007

- 415 Liang, N. and Bougrain, L. (2008). Averaging techniques for single-trial analysis of oddball event-related  
416 potentials. *4th International Brain-Computer*, 1–6
- 417 Lotte, F., Faller, J., Guger, C., Renard, Y., Pfurtscheller, G., Lécuyer, A., et al. (2013). *Combining BCI*  
418 *with Virtual Reality: Towards New Applications and Improved BCI* (Berlin, Heidelberg: Springer Berlin  
419 Heidelberg). 197–220. doi:10.1007/978-3-642-29746-5\_10
- 420 Lowe, G. (2004). SIFT - The Scale Invariant Feature Transform. *International Journal* 2, 91–110
- 421 Madarame, T., Tanaka, H., Inoue, T., Kamata, M., and Shino, M. (2008). The development of a brain  
422 computer interface device for amyotrophic lateral sclerosis patients. In *Conference Proceedings - IEEE*  
423 *International Conference on Systems, Man and Cybernetics* (IEEE), 2401–2406. doi:10.1109/ICSMC.  
424 2008.4811654
- 425 Mak, J. N., McFarland, D. J., Vaughan, T. M., McCane, L. M., Tsui, P. Z., Zeitlin, D. J., et al. (2012). EEG  
426 correlates of P300-based brain-computer interface (BCI) performance in people with amyotrophic lateral  
427 sclerosis. *Journal of Neural Engineering* 9. doi:10.1088/1741-2560/9/2/026014
- 428 McCane, L. M., Heckman, S. M., McFarland, D. J., Townsend, G., Mak, J. N., Sellers, E. W., et al.  
429 (2015). P300-based brain-computer interface (BCI) event-related potentials (ERPs): People with  
430 amyotrophic lateral sclerosis (ALS) vs. age-matched controls. *Clinical Neurophysiology* 126, 2124–2131.  
431 doi:10.1016/j.clinph.2015.01.013
- 432 Nam, C. S., Li, Y., and Johnson, S. (2010). Evaluation of P300-based brain-computer interface in real-  
433 world contexts. *International Journal of Human-Computer Interaction* 26, 621–637. doi:10.1080/  
434 10447311003781326
- 435 Nijboer, F. and Broermann, U. (2009). Brain Computer Interfaces for Communication and Control in  
436 Locked-in Patients. In *Graimann B., Pfurtscheller G., Allison B. (eds) Brain-Computer Interfaces. The*  
437 *Frontiers Collection*. (Springer Berlin Heidelberg). 185–201. doi:10.1007/978-3-642-02091-9\_11
- 438 Novak, D., Sigrist, R., Gerig, N. J., Wyss, D., Bauer, R., Gotz, U., et al. (2018). Benchmarking brain-  
439 computer interfaces outside the laboratory: The cybathlon 2016. *Frontiers in Neuroscience* 11, 756.  
440 doi:10.3389/fnins.2017.00756
- 441 Polich, J. (2007). Updating P300: An integrative theory of P3a and P3b. *Clinical Neurophysiology* 118,  
442 2128–2148. doi:10.1016/j.clinph.2007.04.019
- 443 Ramele, R., Villar, A. J., and Santos, J. M. (2016). BCI classification based on signal plots and SIFT  
444 descriptors. In *4th International Winter Conference on Brain-Computer Interface, BCI 2016* (Yongpyong:  
445 IEEE), 1–4. doi:10.1109/IWW-BCI.2016.7457454
- 446 [Dataset] Ramele, R., Villar, A. J., and Santos, J. M. (2017). P300-dataset rrid scr\_015977. <https://www.kaggle.com/rramele/p300samplingdataset>
- 447 <https://www.kaggle.com/rramele/p300samplingdataset>
- 448 Rao, R. P. N. (2013). *Brain-Computer Interfacing: An Introduction* (New York, NY, USA: Cambridge  
449 University Press)
- 450 Renard, Y., Lotte, F., Gibert, G., Congedo, M., Maby, E., Delannoy, V., et al. (2010). OpenViBE: An  
451 Open-Source Software Platform to Design, Test, and Use Brain-Computer Interfaces in Real and Virtual  
452 Environments. *Presence: Teleoperators and Virtual Environments* 19, 35–53. doi:10.1162/pres.19.1.35
- 453 Riccio, A., Simione, L., Schettini, F., Pizzimenti, A., Inghilleri, M., Belardinelli, M. O., et al. (2013).  
454 Attention and P300-based BCI performance in people with amyotrophic lateral sclerosis. *Frontiers in*  
455 *Human Neuroscience* 7, 732. doi:10.3389/fnhum.2013.00732
- 456 Riener, R. and Seward, L. J. (2014). Cybathlon 2016. *2014 IEEE International Conference on Systems,*  
457 *Man, and Cybernetics (SMC)*, 2792–2794doi:10.1109/SMC.2014.6974351



- 458 Schalk, G., McFarland, D. J., Hinterberger, T., Birbaumer, N., and Wolpaw, J. R. (2004). BCI2000: a  
459 general-purpose brain-computer interface (BCI) system. *IEEE transactions on bio-medical engineering*  
460 51, 1034–43. doi:10.1109/TBME.2004.827072
- 461 Schomer, D. L. and Silva, F. L. D. (2010). *Niedermeyer's Electroencephalography: Basic Principles,*  
462 *Clinical Applications, and Related Fields* (Walters Klutter -Lippincott Williams & Wilkins)
- 463 Sellers, E. W., Kübler, A., and Donchin, E. (2006). Brain-computer interface research at the University of  
464 South Florida cognitive psychophysiology laboratory: The P300 speller. *IEEE Transactions on Neural*  
465 *Systems and Rehabilitation Engineering* 14, 221–224. doi:10.1109/TNSRE.2006.875580
- 466 Tibon, R. and Levy, D. A. (2015). Striking a balance: analyzing unbalanced event-related potential data.  
467 *Frontiers in psychology* 6, 555. doi:10.3389/fpsyg.2015.00555
- 468 Van Drongelen, W. (2006). *Signal processing for neuroscientists: an introduction to the analysis of*  
469 *physiological signals* (Academic press)
- 470 Vedaldi, A. and Fulkerson, B. (2010). VLFeat - An open and portable library of computer vision algorithms.  
471 *Design* 3, 1–4. doi:10.1145/1873951.1874249
- 472 Wolpaw, J. and E., W. (2012). *Brain-Computer Interfaces: Principles and Practice* (Oxford University  
473 Press)
- 474 Yamaguchi, T., Fujio, M., Inoue, K., and Pfurtscheller, G. (2009). Design method of morphological  
475 structural function for pattern recognition of EEG signals during motor imagery and cognition. In *Fourth*  
476 *International Conference on Innovative Computing, Information and Control (ICICIC)*. 1558–1561.  
477 doi:10.1109/ICICIC.2009.161

**Table 1.** Percentage of correctly predicted letters while performing an offline BCI Simulation for the best performing channel for each subject of the public dataset of ALS patients. The spelled words are *GATTO*, *MENTE*, *VIOLA* and *REBUS*. Results obtained with the traditional SWLDA algorithm are also shown for comparison.

Participant	BPC	Character Recognition Rates	
		HIST	SWLDA
1	Cz	35%	45%
2	Fz	85%	30%
3	Cz	25%	65%
4	PO8	55%	40%
5	PO7	40%	35%
6	PO7	60%	35%
7	PO8	80%	60%
8	PO7	95%	90%

**Table 2.** Percentage of correctly predicted letters while performing an offline BCI Simulation for the best performing channel for each subject of the public dataset of ALS patients. The spelled words are *GATTO*, *MENTE*, *VIOLA* and *REBUS*. Results obtained with the traditional SWLDA algorithm are also shown for comparison.

Participant	BPC	HIST	BPC	PE	BPC	SVM
1	Cz	35%	Cz	45%	Cz	90%
2	Fz	85%	Cz	30%	Cz	90%
3	Cz	25%	Cz	65%	Cz	90%
4	PO8	55%	Cz	40%	Cz	90%
5	PO7	40%	Cz	35%	Cz	90%
6	PO7	60%	Cz	35%	Cz	90%
7	PO8	80%	Cz	60%	Cz	90%
8	PO7	95%	Cz	90%	Cz	90%

**Table 3.** Percentage of correctly predicted letters while performing an offline BCI Simulation for the best performing channel for each subject of the own dataset. The spelled words are *MANSO*, *CINCO*, *JUEGO* and *QUESO*. Results obtained with the traditional SWLDA algorithm are also shown for comparison.

Participant	BPC	Character Recognition Rates	
		HIST	SWLDA
1	Oz	40%	65%
2	PO7	30%	15%
3	P4	40%	50%
4	P4	45%	40%
5	P4	60%	30%
6	Pz	50%	35%
7	PO7	70%	25%
8	P4	50%	35%





**Figure 1.** Example of the  $6 \times 6$  Speller Matrix used in the study. Rows and columns flash in random permutations.

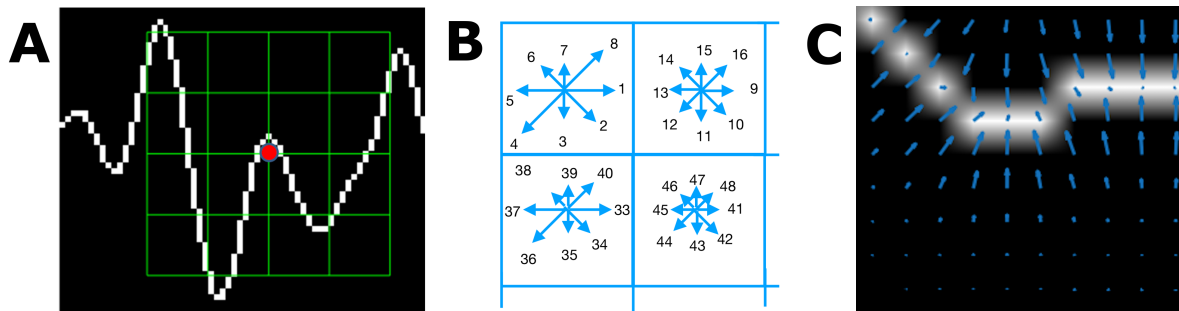


**Figure 2.** (A) Example of a plot of the signal, a keypoint and the corresponding patch. (B) A scheme of the orientation's histogram computation. Only the upper-left four blocks are visible. The first eight orientations of the first block, are labeled from 1 to 8 clockwise. The orientation of the second block  $B_{1,2}$  is labeled from 9 to 16. This labeling continues left-to-right, up-down until the eight orientations for all the sixteen blocks are assigned. They form the corresponding **kp**-descriptor of 128 coordinates. The length of each arrow represent the value of the histogram on each direction for each block. (C) Vector field of oriented gradients. Each pixel is assigned an orientation and magnitude calculated using finite differences.

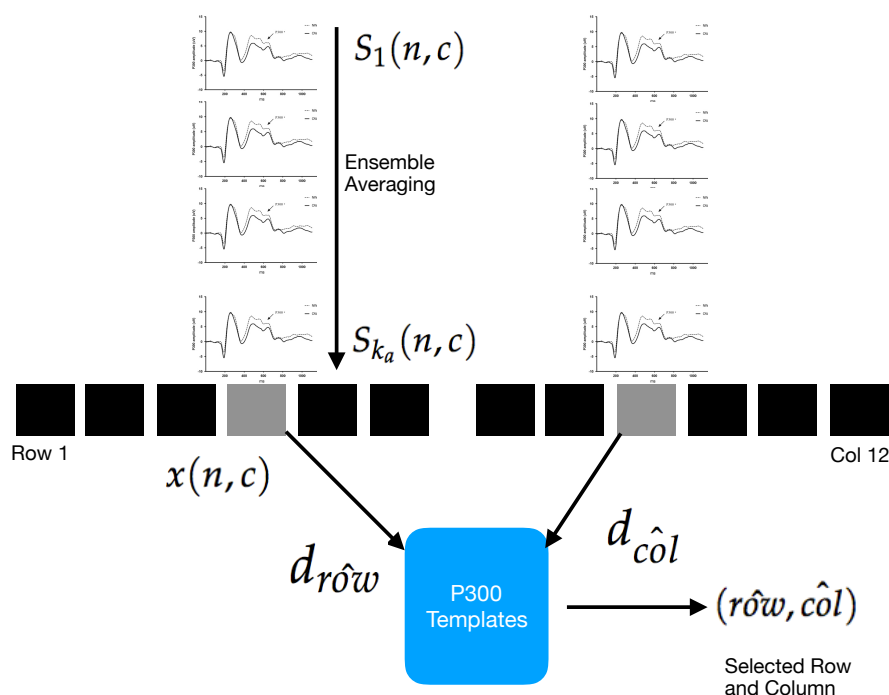


**Figure 3.** Segments  $S_i$  are averaged for the 6 rows and 6 columns. From the averaged signal, the image of the signal plot is generated and each descriptor is computed. By comparing each descriptor against the set of templates, the P300 ERP can be detected, and finally the desired letter from the matrix can be inferred.

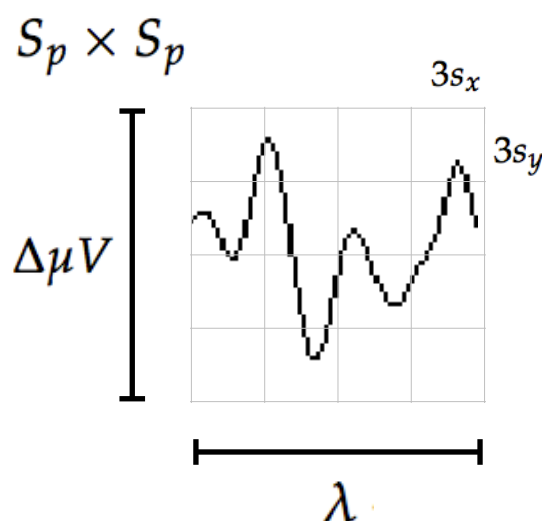


**Figure 4.** The scale of local patch is selected in order to capture the whole transient event. The size of the patch is  $X_p \times X_p$  pixels. The vertical size consists of 4 blocks of size  $3s_y$  pixels which is high enough as to contain the signal  $\Delta\mu V$ , the peak-to-peak amplitude of the transient event. The horizontal size includes 4 blocks of  $3s_x$  and covers the entire duration in seconds of the transient signal event,  $\lambda$ .

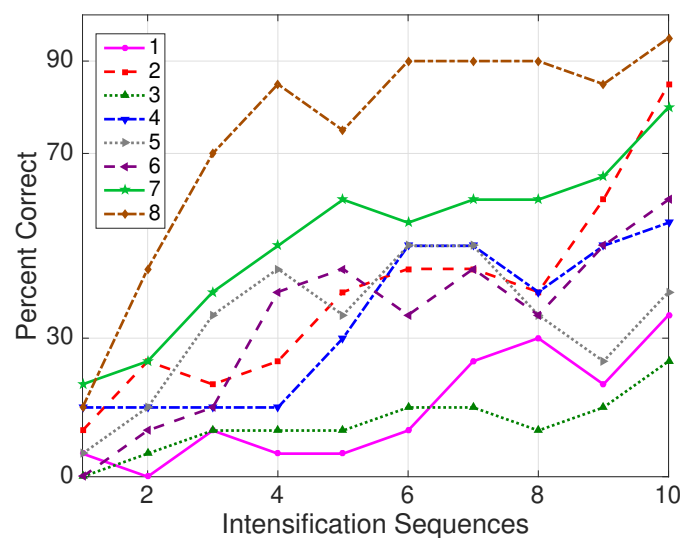


**Figure 5.** Performance curves for the eight subjects included in the dataset of ALS patients. Three out of eight subjects achieved the necessary performance to implement a valid P300 speller.

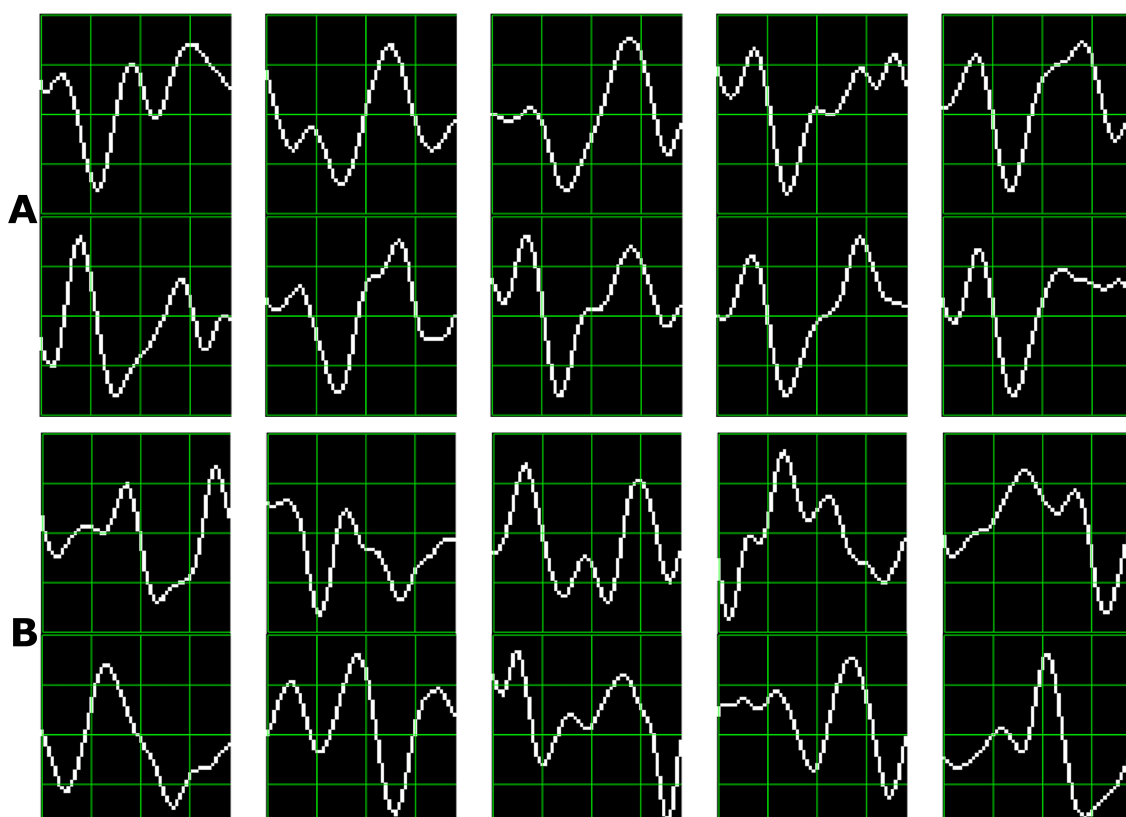


**Figure 6.** P300 template patches for subjects 8 (A) and 3 (B). As traditional done in neuroscience research, downward is positive polarity.